Doctor Thesis

Natural Convection induced by Internal Heat Generation
Yuji Tasaka
(Table of contents) (Introduction)

Master Theses

* Analysis of Vortex Ring in Rotating Field Using UVP
H. Kitaura
(Abstract)
***** Taylor-Couette Flow of Liquid Gallium
Y. Sato
(Abstract)
* Study of Bubbly Turbulent Channel Flow Using UVP
J. Nagao
(Abstract)

Diploma Theses

* Flow Characteristics of Gas-Liquid Two Phase Flow in Inclined Tube
J. Ohashi
He designed and constructed all the equipment to study slug flow structures at a high speed condition, and found that the slug frequency was sensitive to the inclination angle.
* Application of UVP to a Flow Measurement of Rivers
S. Kojima
He established a new method to detect a bottom of a river and developed a program for flow field measurement of a river.
* Generation of Oscillating Grid Turbulence of Liquid Flow
S. Kon
He constructed a rig for generating oscillating grid turbulence and verified a region in which homogeneous turbulence is realized.
* Taylor-Couette Flow of Liquid Gallium
T. Kondoh
He investigated behavior of Taylor vortices at high Reynolds number.
* Wall Turbulence in a Horizontal Bubbly Turbulent Channel
M. Nishimoto
He visualized wall turbulence structure in a channel using Kalliroscope and found that streamwise vortices remained in the vicinity of large bubbles.

Table of Contents

Chapter 1

Introduction

1.1 Preface

Natural convection in a shallow fluid layer makes a beautiful convection pattern at various places, e.g. a cloud pattern in the sky, water circulation in a paddle on the ground after the rain. Such art of Nature certainly has melted someone's heart since ancient times.

Bénard first dealt with this phenomenon as a physical problem in his work [1]. Since his works at early 1900s, it has been continuously investigated as an extremely fundamental phenomenon of a thermal convection appearing in engineering and science fields until now. Rayleigh added a mathematical explanation to a formation of the convection pattern by stability analysis [2]. After that, mathematicians have investigated this phenomenon as a typical problem of a pattern formation and a bifurcation of a solution [3]. In the long history of the investigation, the study of this problem has taken in many elements, e.g. influences of a rotation and a magnetic field [4, 5], effects of surface tension [6, 7], and it putted off great achievements respectively (See Koschmieder (1993) [8]). It has, however, misplaced important elements, "internal heat generation" and "low Prandtl number fluid", on the way.

1.2 Background & literature survey

1.2.1 Internally heated convection

Natural convection induced by internal heat generation exists everywhere in nature. Examples are motion in the atmosphere [9, 10, 11] where heat generation is generated by absorption of sunlight, and mantle convection in the earth [12]–[15] where heat is generated by radioactive decay of isotopes. In the artificial structures, microwave ovens and induction heater such as an electric melter generate internal heat. In the event of hypothetical core meltdown of the nuclear reactor heat generation is internal. There are many systems in which this phenomenon becomes dominant in geophysics and thermal engineering. Recently, the

problems of such internally heated convection are investigated as realistic problems in actual equipments [16]–[20] or in evolution of the earth [21] by mainly using a numerical simulation. Since early 1970s, however, to our knowledge, there have been no fundamental investigations of this problem, and then there are unsolved problems in the internally heated convection.

Despite the importance of internal heat generation, there are few systematic investigations of its effects. Most of previous works have only considered the much simpler case in which heat generation is uniform overall the fluid layer and a thermal boundary condition at the bottom of the fluid layer is adiabatic. For example, Tritton & Zarraga [22] carried out experimental investigations and found various interesting features; formation of irregular, hexagonal cell with descending flow in the center of a cell, transition of convection cell pattern with respect to internal heat generation, particular interest was the dilatation of convection cells with increasing rate of internal heat generation. Schwiderski & Schwab [23] attempted to confirm the features by an improved experimental setup and they concluded that cell dilatation is not an intrinsic feature of the problem, but instead is induced by non-uniformity of internal heat generation in the experimental apparatus. Carrigan also denied the cell dilatation in his experimental works [24, 25] (But he used copper wires as electrodes in order to realize internal heat generation electrically and then heat generation was clearly non-uniform in the fluid layer.). Sparrow *et al.* [26] first dealt with this problem theoretically as a problem of stability of non-linear temperature gradient. Theoretical study by Roberts [27] carried out a linear stability analysis and an estimation of the preferred modes in the finite amplitude convection. Tveitereid & Palm [28] achieved enhanced analyses of Roberts's work. Thirby [29] performed a numerical simulation and compared his result with the theoretical studies. Their studies, however, could not clarify the features mentioned in the experimental studies. They attributed the cell dilatation to non-uniform heat generation due to imperfections in the experiments; that is, a deviation from uniform heating due to a spatially varying electrical conductivity.

As an enhanced model of the internally heated convection, non-uniform distribution of internal heat generation was treated by Krishnamurti [11] in the context of cloud formation in meteorology. Her experiment, however, uses a chemical reaction to simulate the internal heat generation and cannot be easily modeled for analysis. Yücel & Bayazitoglu [10] also investigated a non-uniform distribution theoretically by using a model in which the heat

source increases exponentially from the lower to the upper boundary. Their model, however, was combined with complex boundary conditions which consequently did not allow the fundamental characteristics of heat source distribution to be clarified.

There are the other advanced studies; Internally heated convection in a thermally stratified layer [30], Uniform internal heating with rotation [31, 32], With isothermal boundary condition at the bottom of the fluid layer [33]. Weinstein & Olson [34] performed experimental observation of the convective motion in a mixed heating condition, internal and external heating at the bottom, at extremely high Rayleigh number. They showed a sheet shape descending motion and compared it with their numerical work [35].

1.2.2 Rayleigh-Bénard convection in low Prandtl number fluid layer

Rayleigh-Bénard (R-B) convection, natural convection in a shallow fluid layer induced by heating at the bottom of the fluid layer and by cooling at the top, is a classical problem and has a long history of investigations. These investigations are mainly observation of a convective flow pattern formed in the fluid layer with changing parameters, Rayleigh number and Prandtl number. Figure 1.1 shows a very famous phase diagram of R-B convection drown by Krishnamurti [36]. This diagram shows a transition of the flow pattern with respect to Rayleigh number in the wide range of Prandtl number, where symbols represent results of the observation. The flow pattern changes from steady state to turbulence passing through two-dimensional state, three-dimensional state and time dependent state. Boundaries of these states are expressed by the observation points. There is, however, no observation point in an extremely small side of Prandtl number. As working fluid of low Prandtl number is liquid metal and is opaque, we cannot use optical visualization methods in order to observe the flow pattern.

As first investigation of low Prandtl number R-B convection, Rossby [5] reported time-averaged Nusselt number for mercury layer. Recently, Yamanaka *et al.* [37] measured temperature both in a liquid gallium layer and in a copper block, which is a top plate of the fluid layer, by using a thermocouple in order to correlate convective motion and temporal oscillation of heat flux through the fluid layer. A point measurement of temperature in the fluid layer, however, is not sufficient to clarify the flow pattern in comparison with an optical visualization of the flow pattern.

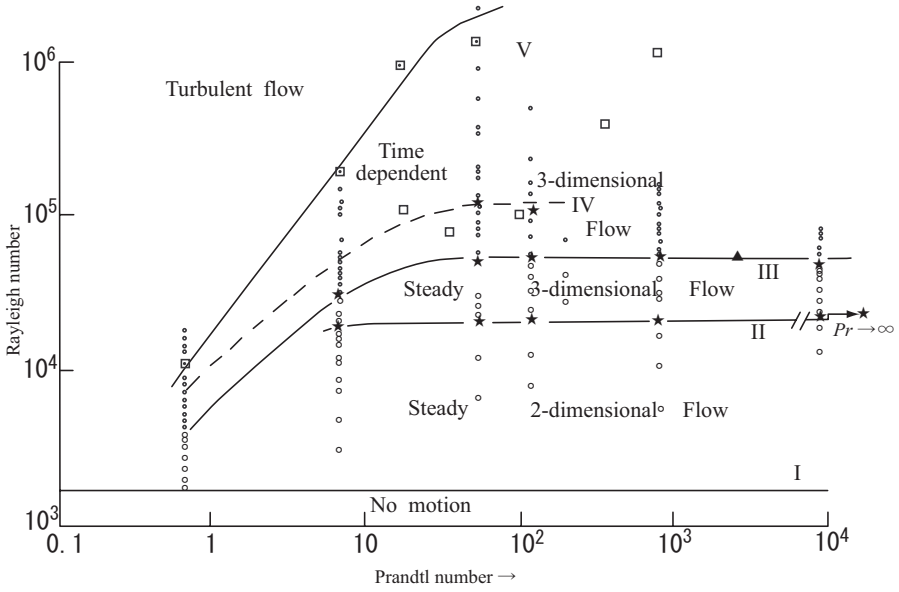

Figure 1.1: The régime diagram for Rayleigh-Bénard convection drawn by Krishnamurti [36].

1.3 Objectives

As a first objective, we focus our study on the influence of the heat source distribution on the convection. As we consider that most of the distribution of the internal heating is caused by absorption of radiating wave such as microwave, an exponential distribution in the vertical direction is assumed. Using a linear stability analysis, we investigate a condition at onset of convection for two cases of the distribution. Secondly, we reinvestigate the remaining problems on internally heated convection, e.g. cell dilatation, and study them in greater detail than conventional visual obserbation allowed. Thirdly, we investigate temperature behavior in the internally heated convection in order to support the qualitative investigation and to compare experimental results and theoretically estimated values quantitatively. Finally, we attempt to measure a velocity profile in a convection layer of liquid gallium by UVP, Ultrasonic Velocity Profiler, in order to visualize a flow pattern in low Prandtl number R-B convection.

1.4 Résumé

This thesis consists of six chapters including Introduction and four appendixes in which results of supplemental experiments and visualized photographs except for photographs appearing in the main chapters. As each chapter excluding Introduction and Conclusion is individually submitted to various journals, they have Abstract, Introduction and Conclusion part. Contents of the main chapters are summarized as follows.

In Chapter 2, the effects of heat source distribution on natural convection induced by internal heating are studied. Simple models of heat source distribution in which the distribution decayed exponentially from the bottom or top boundary were studied. A linear stability analysis was carried out to calculate the critical Rayleigh number and critical wavenumber for the onset of convection. Our results show the influence of the biased heat source distribution on the onset of convection and the effect of the thickness of the source distribution on the size of the convection cell. As a more realistic problem, the effect of additional bottom wall heating on the internal heat driven convection was studied. We show that the parameter controlling the shape of the temperature profile can be expressed as the ratio of the internal to external Rayleigh numbers (where the internal Rayleigh number is defined for internal heating and the external Rayleigh number is defined for wall heating). We found that an asymmetry in the velocity profile appears when there is a local stable layer with a positive vertical temperature gradient.

In Chapter 3, characteristics of internally heated convection, for instance convection cell dilatation, are reexamined using new experimental methods and an improved experimental apparatus in order to reduce uncertainties as much as possible. The convective motion in the fluid layer was visualized using reflecting particles (Kalliroscope) and independently using a suspension of Thermo-chromic Liquid Crystal; the latter technique also allowed the simultaneous investigation of the temperature field. Cell dilatation was conformed in the improved experimental apparatus and then investigated quantitatively by extracting the pattern wavenumber from Fourier analysis of the images recorded by a digital camera. The pattern wavenumber was found to decrease with increasing Rayleigh number. We compare our results with earlier investigations and discuss the influence of the thermal boundary condition at the bottom of the fluid layer on the variation of the wavenumber. Furthermore, we also discussed a reason of disagreement between theoretical and experimental results.

In Chapter 4, temperature behavior in the internally heated convection is quantitatively investigated. Calibration system was developed in order to convert the visualized photographs of temperature field obtained in Chapter 3 to real temperature field. Calibration curve correlating color information extracted from the photograph to temperature is determined from approximately linear temperature distribution in horizontal fluid layer by hue method. The photographs taken at various internal Rayleigh numbers are converted to temperature field by the obtained curve. A temperature profile in a cell is analyzed by extracting individual cell from a temperature field and we discussed variation of the profile with respect to internal Rayleigh number. Statistical values of the temperature field are compared with theoretically estimated values, and they are well related.

In Chapter 5, we attempt to measure a velocity profile in a convection layer of liquid gallium by UVP, Ultrasonic Velocity Profiler, in order to visualize a flow pattern in low Prandtl number R-B convection. Trial UVP measurements were performed in a fluid flow of liquid gallium driven by magnetic force and in thermal convection of glycerol solution as a test of a low velocity flow measurement. These results confirm a validity of UVP measurement on the convective motion in liquid gallium layer. An experimental apparatus of liquid gallium convection suitable for UVP measurement was developed. We could measure the velocity profile successfully and measure it at different position or at various Rayleigh numbers. These results visualize a convection pattern in the layer and show a temporal behavior of the pattern.

1.5 Nomenclature

c	:	sound speed
c_p	:	specific heat
g	:	gravity
H	:	volumetric heat source
H_0	:	total power deposited
k	:	horizontal wavenumber
k_c	:	critical wavenumber
L	:	height of the fluid layer
p	:	pressure
Pr	:	Prandtl number
q	:	distribution function of internal heat source
R_I	:	internal Rayleigh number
R	:	external Rayleigh number
R_c	:	critical Rayleigh number
R_I^*	:	reduced internal Rayleigh number, $R_\mathrm{I}^* = R_\mathrm{I}/R_\mathrm{c}$
t	:	time
T	:	temperature
$\boldsymbol{u}(u,v,w)$	:	velocity vector and its components
$\boldsymbol{x}(x,y,z)$	:	coordinates of position
β	:	bulk modulus
ΔT	:	temperature difference between the top and the bottom boundaries
ε, η	:	characteristic length of heat source distribution
Θ	:	$= R_\mathrm{I}/R$
λ	:	thermal conductivity
κ	:	thermal diffusivity
μ	:	viscosity
ν	:	dynamic viscosity
ρ	:	density
$*$	:	dimension variable (In Chapter 2)
$\hat{}$	:	perturbation
$\tilde{}$	:	amplitude function of perturbation

Abstract

This study is a collaboration research between LFC of Hokkaido University and Fluid Dynamics Group of University of Warwick in U.K. Our research team visited the laboratory at University of Warwick on March and September in 2004 and carried out experiments there. I appreciate them so much for their kind cooperation and fruitful discussion.

A vortex ring can be seen in various natural and industrial situations for handling intermittent fluid flow such as volcanic fumes, smoke rings, and fuel injection systems. It is often chosen as a suitable research target to obtain fundamental knowledge on flow transition or instability caused by nonlinear phenomena. A dynamics of a flow in a rotating field is studied in the area of geophysical and industrial applications such as a centrifugal separator. Our interest is to know how a background rotation provides the effect on motion and structure of the vortex ring. In this study, UVP (Ultrasonic Velocity Profiler) is used to acquire the differences of structure with and without a background rotation from the two-dimensional flow field, which is measured by three ultrasonic transducers. In this paper we mention on the reconstruction method and the difference of ring structure with and without background rotation in the view of vorticity distribution.

A vortex ring is emitted downward from a vortex ring generator fixed on the top of a water tank with 2 m height and 1 m width. The tank is placed on a large rotating table, whose angular velocity is 2.5 rpm. The vortex ring generator is composed of a cylindrical nozzle and a reciprocating piston. The diameter of nozzle D_0 is 50 mm and the piston to push out the vortex ring is connected with a stepping motor controlled by computer, so the stroke S_p and the piston speed V_p are variable to be controlled. In our experiments we chose S_p = 50, 90, 130 mm and V_p = 100, 300, 500 mm/s. Three ultrasonic transducers are fixed in the tank as shown in Fig.3.6 (p.15). The transducer A is arranged upward on the axis of the nozzle to measure the vertical velocity distribution from which a position of the vortex ring can be traced. The transducer B and C are fixed horizontally and 45 degree downward respectively to measure the inner velocity profiles of the vortex ring passing through each measurement line. Three measurement lines cross at a point located 250 mm downstream from the nozzle tip. The measurable range from the cross point is 100 mm for all transducers. Hydrogen bubbles as fluid tracers are generated below the test section. The hydrogen bubble generation is realized based on a water electrolysis using platinum wire and aluminum bar connected with 30V DC power supply.

The translational velocity of vortex ring is obtained from the advection velocity of the vertical velocity profiles measured by the transducer A. Fig.5.11 (p.35) shows a sample of time evolution of the vertical velocity profile moving downward. This profile gives instantaneous positions of vortex ring. The translational velocity U_T is determined as the slope as shown in Fig.5.11. Fig.5.12 (p.37)

shows the results of U_T as the function of V_p and it shows that U_T increases with V_p and S_p, and that U_T with background rotation is lower than without rotation.

The two-dimensional flow field of the vortex ring can be reconstructed by combining multiple measurement data from different alignment of ultrasonic transducers, transducer B and C. Fig.5.5 (p.28) and Fig.5.8 (p.32) show the results of the spatio-temporal velocity profile. As shown in Fig.5.13 (p.39), translational velocity can be estimated geometrically from the result of transducer C on the assumption that the vortex ring translates at a uniform velocity and keeps its flow structure while it passes through the measurement line. Therefore temporal coordinate in Fig.5.5 and Fig.5.8 can be translated to spatial coordinate by using the translational velocity. Furthermore, we must fit the each position of two velocity profiles because they have different spatial coordinates each other. After the “spatial fitting”, the velocity vector can be calculated geometrically from Eq.5.2 and Eq.5.3 (p.39) as shown in Fig.5.15 (p.41). Fig.5.17 to Fig.5.20 (pp.44-47) show the results of relative velocity vector field and vorticity distribution, which is similar to the Gaussian distribution. In this study we define the vertex core as the region whose vorticity is larger than a half of the maximum vorticity in order to evaluate the effects of the background rotation to the vortex ring structure quantitatively. Fig.5.23 (p.52) and Fig.5.24 (p.53) show the standardized vorticity distribution in and around the core without and with the background rotation.

The total circulation Γ, which is obtained as the sum of the vorticity on the cross-section, decreases in the rotating field as shown in Fig.5.25 (p.54). On the other hand the core circulation Γ_C, which is obtained as the sum of the vorticity in the core, is almost fixed. It means that the vorticity is concentrated in the vortex core by the effect of background rotation, $\Gamma_c/\Gamma = 0.4$ without background rotation and $\Gamma_c/\Gamma = 0.6$ with background rotation as shown in Fig.5.26 (p.55). It seems that the vorticity reduction is caused near the axis of the rotation out of the vortex core. Verzicco et al, who studied in larger rotational condition, reported that the secondary vorticity of opposite sign is generated there and the vortex ring is stretched radially by the interaction with it. A stretching of the vortex ring causes an increase of the local vorticity in the core and a reduction of the cross-section of the core. Therefore, the viscous diffusion is enhanced because vorticity gradient is steeper. In this study vorticity concentration is also seen in the smaller rotational conditions, so we think viscous diffusion is enhanced.

Summarizing our study, the flow structure of the vortex ring has been successfully measured using UVP applied to three measurement lines. 1) From the velocity profiles measured by transducer A, instantaneous translational velocity can be discussed and it indicates that the vortex ring translates with unique velocity with respect to the piston speed and stroke on our test section and that in rotating field translational velocity decreases. 2) By combining the velocity profiles measured by transducer B and C, two dimensional velocity vector field and vorticity distribution on cross-section

are obtained and they indicate that the background rotation enhances viscous diffusion of vortex ring because of the vorticity concentration inside the vortex core.

Abstract

The flow between coaxial rotating cylinders is called Taylor Couette flow. A flow transition in this configuration with only inner cylinder rotation was investigated using ultrasonic Doppler profiler (UVP) for the range of Reynolds number R up to 100 times critical Reynolds number (R_c). At very low Reynolds number, the flow is circular Couette flow. At $R = R_c$, Taylor vortices appear, which is three-dimensional time-independent axis-symmetric counter-rotating vortices. On increasing R, azimuthal waves appear and instability sets in. On further increasing R the azimuthal waves disappear, and then the flow is turbulent although the Taylor vortex structure remains. Another investigation was performed by Lathrop *et al*. with torque measurement. Fig.1.7 (pp.6) shows a variation of the local exponent for the torque. The gradient changes at around R^*~160-200. It suggests the structure of the flow changes at this region.

No investigation has been performed for the range of longer than 100 times R_c using UVP because of the limit of the measurable velocity range. We use liquid gallium as the working fluid to solve this problem. Liquid gallium has low kinematic viscosity, high sound speed, and low melting temperature. Low kinematic viscosity makes high R with even low fluid velocity. High sound speed makes the maximum measurable velocity higher. And, it's easier to work and control the substance condition in a laboratory than other liquid metal. However, it's difficult to measure velocity of liquid metal. Liquid metal has a strong link with industry such as iron and steel industry. So it's also important to develop measuring method for liquid metal.

Tracer particle is needed in the working fluid with UVP measurement. We selected zirconium boride powder as the tracer, which has almost the same density as gallium and is a stable substance. It's difficult to mix the tracer particles in gallium because the surface tension of liquid metal is very high. We mix the tracer particles in gallium at a temperature of 500 °C by reducing the surface tension.
Another problem was that gallium is very easy to be oxidized. Most process was done under an oxygen-free atmosphere, and oxidized gallium was deoxidized with 10 % solution of HCl in ethanol.

Fig.2.11 (pp.14) shows the experimental set up. The coaxial rotating cylinder system in this experiment has the same radius ratio $\eta = r_i/(r_i + d) = 0.919$ and aspect ratio $\Gamma = L/d = 20$ as that of earlier water experiment with UVP to compare the results (r_i is the radius of inner cylinder: 114 mm, d is the gap distance: 10 mm, L is the height of fluid layer: 200 mm). The inner and outer cylinders are made of copper to get good wetting with liquid gallium. UVP measures instantaneous velocity profile parallel to the axis of the cylinder. The ultrasonic (US) basic frequency is 4 MHz. The ultrasonic transducer is set near the outside wall of the gap. Reynolds number is defined as $R = d\,\Omega\, r_i / \nu$ (Ω is angular velocity, ν is kinematic viscosity). Reduced Reynolds number is defined as $R^* = R/R_c$ ($R_c = 134.57$).

The experimental condition is shown in table 2.4 (pp.23), for the range of $44<R^*<396$. In Run 1-4, we obtained velocity profiles at each R^* continuously to investigate the behavior of stable Taylor vortex. In Run 5-10, we measured at each R^* intermittently to investigate the most stable shape of Taylor vortex.

Fig.3.1 (pp.24) shows an example of measured velocity fields. The average velocity distribution is shown in fig.3.2 (pp.24). The horizontal bands correspond to each roll of TVF and, explain a Taylor vortex. Fig.3.7 (pp.29) shows an example of time dependent space domain energy spectra. And fig.3.8 (pp.30) shows the averaged energy spectra. The non-dimensional wavelength of Taylor vortex λ^* is estimated from the wave number at the peak point. Fig.4.3 (pp.34) shows the variation of the λ^* on increasing R^*. At the range of $100<R^*<200$, the value of λ^* is higher than the other range of R^*. At the higher R^* than 200, the value of λ* is almost constant and higher than that at low R^*. Thus the flow might have a kind of transition region at $100<R^*<200$, and the most stable value of λ^* is changed after this region. This result agrees with that reported by Lathrop. To pay attention to the result of Run 1-4, the value of λ^* is almost constant in each Run. It explains that Taylor vortex is stable against change of R^*. Fig.3.10 (pp.36) shows an example of time domain power spectra, and fig.3.11 (pp.37) shows the averaged power spectra. There is no peak and characteristic shapes in power spectra at all R^* studied here. It explains that the flow has no azimuthal wave structure in Taylor vortex.

In conclusion: We developed the measurement method of liquid gallium flow and established the experimental apparatus for Taylor Couette flow of liquid gallium. We obtained the time series of velocity distribution of Taylor Couette flow at high R^*. The flow might have a transition region at $100<R^*<200$, and the most stable value of λ^* is changed after this region. This supports the past investigation. Taylor vortex is stable against change of R*. The flow has no azimuthal waves structure in Taylor vortex for the range of $44<R^*<396$.

Abstract

Frictional drag reduction for large ships is important for cost-saving, speeding-up, and environmental problem. A method by mixing microbubbles into a turbulent boundary layer is known as a one of effective and ecological techniques. The mechanism of drag reduction with this method is however not clarified comprehensively. The aim of the present study is to elucidate it experimentally. We treat bubbles with about 2 to 30 mm in diameter, which is rather practical than so-called microbubbles due to power saving for the bubble generation. There are two objectives set in this study. One is to establish the measuring method of single-phase turbulent channel flow using UVP (Ultrasonic Velocity Profiler) as well as to evaluate the wall shear stress from the mean velocity profile measured. The second is to apply the UVP to bubbly two-phase flow.

A horizontal channel employed in this study has 6000 mm length, 160 mm width, and 40 mm height(=H). Measuring position of UVP is 2100 mm downstream from the entrance of the channel, where the flow is confirmed as fully developed turbulent flow. Working fluid is water, and reflection particle for ultrasound for measurement by UVP is Diaion, which is styrene benzene copolymer. Bubbles are generated by a bubble generator, which has 13 injection needles. Flow rate controlled by a pump ranges from 120 to 200 *l* / min. Reynolds number is defined as $Re = U_m H/ \nu$, where U_m is mean velocity and ν kinetic viscosity. Air flow rate ranges from 0 to 10 *l* / min. Experimental conditions are Re = 13000 to 54000 and void fraction α changing from 0 to 0.06.

Fig.3-1 shows mean velocity profile of single-phase flow at each *Re*, where they are well corresponding with theoretical value, 1/7 law (Fig. 3-5). It is confirmed that single-phase flow can be measured correctly by UVP and the wall law is applicable to the channel flow. Frictional velocity can be estimated from a mean velocity profile by a logarithmic low using least square approach. Wall shear stress and wall friction factor are calculated from the estimated frictional velocity, and it is confirmed that the latter is well corresponding to Blasius's equation.

Reynolds stress contributes largely to shear stress in the turbulence in a single-phase flow, thus we calculate it from the both of the wall shear stress and the mean velocity profile, excluding the case of bubbly flow. Thus, Reynolds stress in two-phase media should be measured directly. A velocity vector measurement is accomplished using 2 US transducers aligned at different angles. The measured Reynolds stress shows the same tendency with theoretical value excluding a magnitude. One of the reasons of the error is expected as the expansion of the measurement volume caused by expansion of ultrasonic beam. Fluctuation of velocity, which causes Reynolds stress, is averaged in the large measurement volume, and then it becomes smaller. The other reason may be that 2 US transducers cannot realize perfectly co-instantaneous velocity measurement. The alternative method to overcome this matter is to use focusing transducer, which is under development in our laboratory.

Bubbly flow itself is difficult to measure exactly using commercial UVP system, because large part of ultrasonic wave is reflected at the gas-liquid interface. Fig.4-6 shows a color map of spatio-temporal velocity distribution of single-phase flow and bubbly flow. In the case of bubbly flow, locally small velocity regions exist near the top wall. It may be caused by bubble interface passing in the measurement line. It gives a wrong mean velocity profile at y / H = 0.8 (Fig.4-2 and Fig.4-3). A method to remove such as wrong profile objectively and automatically is established using following thresholding techniques. 1) An instantaneous, streamwise velocity in the channel flow must be positive, thus a negative instantaneous velocity is assumed as wrong data induced by passing bubbles. 2) A velocity fluctuation induced by bubble passing becomes larger beyond $u \pm \sigma$, 2σ (u is mean velocity and σ is standard deviation of u). After performing these methods, mean velocity profile of liquid phase is calculated by remaining data, but they have a tumble (Fig.4-8 and 4-10), namely these methods did not work realistically. Eventually, we try to discriminate the velocity map based on image processing. On a color map of a spatio-temporal velocity distribution, suddenly velocity changes when bubble passes on the measurement line. Derivation filter (Fig.4-11) may be able to emphasize such a large velocity gradient, which corresponds to bubble interfaces. Fig.4-12 shows the result of performing the derivation, where large derivative value regions exist near the top wall, which does not seen in single-phase flow. Namely, bubble surface is emphasized correctly. Position of bubble surface is determined objectively by binarizing these derivative values using proper threshold. Two algorithms, i.e. Otsu's method and P-tile method, determine the threshold.

Fig.4-14 shows determined bubble surface. Blue area on the color map corresponds well with observation. The mean velocity profile of liquid phase calculated from profiles excluding bubbles is shown in Fig.4-15. In these figures, almost of these profiles do not have tumble due to bubbles, thus the discrimination of the profile bubble passing was succeeded. In these figures, mean velocity profiles become flatly in the region above y / H =0.8, where is surrounded by bubbles. This is attributed to the fact that 1) bubbles flow slower than the mainstream, so the liquid-phase flows as the same speed as bubbles in the bubbly layer, 2) the velocity gradient of the region becomes moderately because bubbles do not change the shape drastically in a short time. It is known that the Reynolds stress is proportional to velocity gradient squared in the model of mixing length, therefore it will be decreased in the region surrounded by bubble. This will be one of possible reason of frictional drag reduction achieved by large bubbles inside a wall turbulent boundary layer.